Evolution of the Zonal Mean State in the Equatorial Middle Atmosphere during October 1978–May 1979

MATTHEW H. HITCHMAN AND CONWAY B. LEOVY

Department of Atmospheric Sciences, University of Washington, Seattle, WA 98195

(Manuscript received 2 January 1986, in final form 17 July 1986)

ABSTRACT

The evolution of the zonal mean state in the equatorial middle atmosphere is investigated with the use of daily mapped temperatures derived from the Limb Infrared Monitor of the Stratosphere (LIMS) experiment. These quasi-global, high vertical resolution data cover the pressure range 100–0.05 mb and the period 25 October 1978–28 May 1979. The equatorial semiannual oscillation (SAO) in zonal mean temperature, derived zonal wind and meridional shear of the zonal wind is described in detail. Rocket profiles are used to validate features seen in LIMS data. These include ranges in temperature and zonal wind of 20 K and 100 m s^{-1}, and cross-equatorial shears of at least 3 day^{-1}.

Consistent with the theory that the wave–mean flow interaction is essential to the SAO, flow accelerations over the equator exhibit strong week-to-week variations. While easterly accelerations are moderate and occur in deep cool layers, westerly accelerations are generally stronger and occur in shallow warm layers which descend with time at a mean rate of about 0.3 cm s^{-1}.

A detailed heating algorithm is used to estimate residual circulations. Wave-driven residual mean circulation cells associated with the SAO are found to extend well into midlatitudes, their latitudinal scale expanding from December through February as newly formed SAO westerlies descend in the lower mesosphere. In the descending branch of the SAO circulation over the equator, estimated downward advection is very similar to observed westerly acceleration in pattern and magnitude. Cross-equatorial shear and mean meridional wind both maximize beneath the descending zero wind line, which is also the level of maximum penetration of easterlies into the winter hemisphere. Inertial instability may enhance meridional circulations, especially during November through mid-January in the lower mesosphere. The vertical distribution of wave driving over the equator, inferred as a residual in the zonal momentum equation, is compatible with expectations from gravity wave theory.

1. Introduction

During the last 20 years the equatorial middle atmosphere has been the site of discovery of many unexpected dynamical phenomena, including the strong semiannual variations in the zonal mean state (SAO) prevalent in the altitude range 30–90 km. Until very recently, rocketsonde and nadir satellite data have been the chief sources for an observational description of these variations. The latitude and time resolution of rocket profiles is limited, however, while nadir-viewing radiometers cannot resolve phenomena with vertical wavelengths smaller than ~20 km. The Limb Infrared Monitor of the Stratosphere (LIMS) instrument, active aboard the Nimbus 7 spacecraft during 25 October 1978–28 May 1979, has provided a uniquely detailed picture of the temperature structure of the equatorial middle atmosphere. The LIMS dataset combines the advantages of rocket and nadir-sounder data: high vertical resolution (~3 km) and daily quasi-global coverage. These properties enable derivation of wind fields which are reliable even at low latitudes.

Monthly mean values have traditionally been used in documenting flow evolution in the equatorial middle atmosphere above 30 km. This has led to a description in terms of semiannual, annual and time mean components. A semiannual harmonic need not be directly related to a single sinusoidally varying forcing mechanism. We will use the term SAO in a broader sense, where a spectrum of variations, including important week-to-week components, are considered to be aspects of a cyclic evolution of the flow field with about a 6-month period. In contrast, the term SAO harmonic will be reserved for phases and amplitudes computed from a harmonic analysis of monthly mean data. The nature of our data forces us to examine only one SAO cycle, but it has the advantage of allowing a very detailed analysis of that cycle. The particular details of this cycle are likely to be different from those of other cycles. We therefore emphasize the underlying mechanisms that emerge from studying this detailed record.

The week-to-week variations of the zonal mean SAO are strongly suggestive of forcing by wave driving. Both Rossby waves and Kelvin waves vary on these time scales. In order to gain insight into the mechanisms of the SAO, we use a detailed radiative algorithm to derive the zonal mean diabatic circulation. This is a very good approximation to the residual mean circulation, and our calculation allows us to estimate all terms in the residual mean zonal momentum equation except the

wave driving terms. The time and altitude dependence of these terms is deduced as a residual. An independent assessment of wave-driving based on observed eddy quantities will be reported in a future paper.

A concise review of previous observations of the equatorial middle atmosphere is given in section 2. LIMS temperatures and derived wind fields have been exhaustively validated by comparison with rocket soundings. The characteristics of LIMS and rocket data are described in section 3. The evolution of the zonal mean state at low latitudes and the relationship with extratropical changes during the LIMS data period are described in section 4. Advection by the residual mean circulations is discussed in section 5. The low-latitude winter hemispheric flow structure is found to satisfy the inviscid criterion for inertial instability. In section 6 the possible role of inertial acceleration in "spinning up" mean meridional circulations is explored. Section 7 contains concluding remarks.

2. Background

a. The observed equatorial SAO

The equatorial SAO was discovered by Reed (1962) in radiosonde temperature data, which extend to 10 mb. Reed (1966) subsequently used rocket zonal winds to describe the SAO in the altitude range 28–64 km. More recently, Hirota (1978) and Hamilton (1982) used special rocket data with vertical coverage reaching 75–90 km. The rocket and radar-meteor zonal wind studies of Kantor and Cole (1964), Quiroz and Miller (1967), Groves (1972), Belmont et al. (1974, 1975), and Hopkins (1975) have also contributed greatly to the following picture of flow structure and evolution.

Substantial vertical variations occur in the time mean profile of equatorial zonal wind. Time mean westerlies prevail in the lower mesosphere, reaching $\sim$20 m s^{-1} near 65 km, while easterlies prevail elsewhere, maximizing near 35 km (~ -10 m s^{-1}) and near 85 km (~ -20 m s^{-1}). The annual cycle has largest amplitude ($\sim$10 m s^{-1}) near the stratopause and mesopause, with strongest equatorial easterlies during Northern Hemisphere winters. The SAO harmonic westerlies exhibit continuous downward phase progression from 90 to 30 km at a rate of about 10 km/mo. At the mesopause maximum, westerlies occur near the solstices. They occur at the stratopause about one month after the equinoxes. The SAO harmonic amplitudes are largest ($\sim$30 m s^{-1}) near the mesopause and stratopause, with very small amplitudes near 65 km and below 30 km.

Continuous downward phase progression of actual westerlies from the mesopause to the stratopause is not always observed. Time mean easterlies occur where the SAO and annual harmonics maximize. Because SAO and annual harmonics are very small in the lower mesosphere, where time mean westerlies exist, separate mechanisms are probably responsible for stratopause easterlies and for mesopause easterlies (Dunkerton, 1982).

The view taken in this paper is similar to that of Quiroz and Miller (1967). By presenting time series of zonal wind profiles rather than harmonic amplitudes and phases, they emphasized the complexity of the actual evolution of the zonal wind. During 1966 the range in zonal wind near the stratopause at Ascension Island was 125 m s^{-1}, in contrast with the SAO harmonic amplitude of $\sim$30 m s^{-1}. There is a similar difference between SAO harmonic temperature amplitude and the range in LIMS and contemporaneous rocket temperature profiles which have not been monthly averaged.

The SAO temperature harmonic reaches maximum amplitudes of 2–3 K near 40 km and 2 K near 80 km. Results from studies using rocket temperatures (Cole, 1968; Angell and Korshover, 1970; Groves, 1972; Nastrom and Belmont, 1975; Koshelkov and Butko, 1980) agree well with those from studies using nadir satellite temperatures (van Loon et al., 1972; Barnett, 1974; McGregor and Chapman, 1978; Crane, 1979). High temperatures occur at 60 km near 1 February and 30 km near 1 May, preceding maximum westerlies by 20–60 days. Consistent with the likelihood of separate mechanisms for the stratopause and mesopause SAO, in the layer 50–60 km, SAO harmonic temperature amplitudes are smaller than 1 K and phase progression is variable.

b. Relationship with extratropical circulations

A semiannual variation in temperature and zonal wind also occurs at high latitudes. The SAO temperature harmonic amplitudes are largest near 40 km ($\sim$10 K at 80°N and $\sim$5 K at 65°S) and near 80 km ($\sim$20 K near both poles). There is no coherent vertical phase progression and amplitude minima occur near 30°S and 30°N (Groves, 1972; Nastrom and Belmont, 1975; McGregor and Chapman, 1978; Crane, 1979). Highest temperatures near 40 km occur at the solstices, at which time temperatures are lowest near 80 km. The high latitude SAO near 40 km may be accounted for by the summer radiative maximum plus a secondary winter maximum due to Rossby wave driving (Barnett, 1974).

Near each winter solstice, low and high winter latitudes appear to be coupled. Temperature trends on the time scale of Rossby wave-driving that occur in the polar winter stratosphere are accompanied by trends of the opposite sign in the polar mesosphere and equatorial stratosphere, and of the same sign in the equatorial mesosphere (van Loon et al., 1972; Hirota and Barnett, 1977; Chandra, 1985; Al-ajmi et al., 1985). The spatial pattern of temperature changes during a winter polar stratospheric warming is compatible with large-scale residual mean circulations having vertical divergence near the high latitude stratopause, poleward flow in midlatitudes and vertical convergence at low

latitudes extending into the summer hemisphere. As illustrated in Fig. 1a, Rossby wave-driving near the midlatitude stratopause could produce such a pattern.

c. *Comparisons between the QBO and SAO*

Below 30 km the dominant pattern of flow evolution in the equatorial stratosphere is the quasi-biennial oscillation (QBO). Alternating layers of easterlies and westerlies form and descend with time, the pattern repeating every 22–34 months (Coy, 1979). Plumb and Bell (1982) have shown that QBO temperature perturbations have meridional circulation cells associated with them and that these circulations affect the rate of descent of shear zones. Figure 1b illustrates the effects of Kelvin and westerly gravity wave absorption, over the equator. Wave driving by Kelvin and gravity waves is the likely cause of equatorial SAO westerlies (Lindzen and Holton, 1968; Hirota, 1978; Hayashi et al. (1984), Coy and Hitchman (1984). The resulting induced residual mean circulations will contribute to the descent of a westerly shear zone.

Temperature and zonal wind amplitudes are similar for the SAO and QBO, but the descent rate of the SAO zero wind line is about ten times faster. Because the radiative damping rate is greater at the higher altitudes of the SAO, stronger subsidence velocities are required to maintain a given positive temperature anomaly. Moreover, the poleward extend of QBO circulation cells is ~15°–20°, while it is ~30°–40° for the SAO. Thus, it will be argued that larger, more vigorous residual mean circulations are associated with the SAO and that advection plays a more important role.

Using radiosonde data with high latitudinal resolution, Hamilton (1984) and Dunkerton and Delisi (1985) have shown that the initial westerly acceleration of the QBO is concentrated within a few degrees of the equator. A similar feature occurs in the LIMS data for the descending SAO westerlies. In section 5b a possible explanation will be offered.

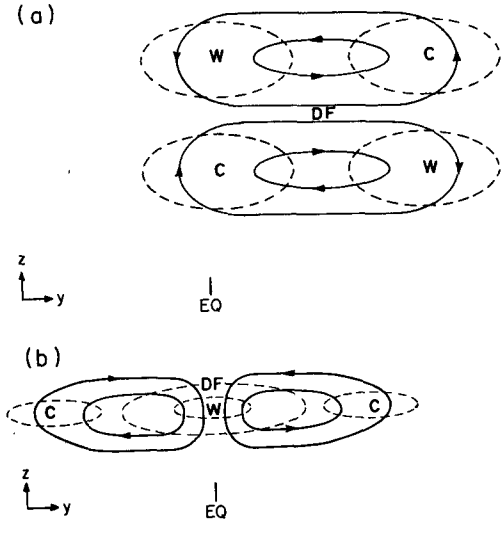

FIG. 1. Schematic diagrams of temperature anomalies and meridional circulations associated with (a) easterly wave driving and (b) westerly wave driving, centered near "DF", after Plumb and Bell (1982).

3. Data and analysis

a. *LIMS data*

The LIMS experiment has been described by Gille and Russell (1984). Gille et al. (1984) compared individual temperature retrievals with approximately contemporaneous and co-located rocket and radiosonde profiles, and described possible sources of systematic error. Absolute accuracy is thought to be better than 2 K in the pressure range 100–1 mb. Precision is better than 0.6 K in the 100–0.1 mb layer.

The most useful product to study synoptic features is the set of mapped temperature fields, which was derived from the individual profiles using the Kalman filter sequential estimation technique (Rodgers, 1976). In making mapped fields, the profiles of temperature values at irregular pressure levels were interpolated to the 18 standard levels 100, 70, 50, 30, 16, 10, 7, 5, 3, 2, 1.5, 1.0, 0.7, 0.5, 0.4, 0.2, 0.1 and 0.05 mb (a spacing of about 3.5 km). These were binned in 4 degree boxes from 64°S to 84°N. For each latitude and pressure level 13 harmonic coefficients (the zonal mean plus the sine and cosine coefficient for the first six zonal wavenumbers) were updated for each new data value. Both ascending and descending orbital data were used. The Kalman filter interpolates coefficients to synoptic times 1200 GMT.

Two main profile inversion algorithms have been used, resulting in some differences for phenomena with vertical scales smaller than ~20 km. LIMS versions one–four (V1–V4) were created at the National Center for Atmospheric Research (Bailey and Gille, 1986). Version five (V5) was created at the Langley Research Center (Gordley and Russell, 1981; Remsberg et al., 1984a; Gordley et al., 1986, manuscript in preparation). Due to superior results for constituent fields, the V5 version was archived by the LIMS Nimbus Experiment Team. Version V5 mapped ozone values are used in the heating algorithm described in section 3d.

An extensive comparison of V4 and V5 mapped temperatures and derived zonal winds with rocket temperatures and zonal winds was carried out for the purpose of determining the relative utility of V4 and V5 data in studying zonal mean and wave quantities in the equatorial middle atmosphere (Appendix B, Hitchman, 1985). In general the V4 and V5 mapped datasets are very similar. When atmospheric phenomena vary slowly in space, as is typical of extratropical latitudes, rocket-V5 agreement is somewhat better in the range 50–0.5 mb. However, when rocket profiles exhibit strong variations in the vertical, as in the strong

westerly shears of the SAO, the features are represented significantly better by V4 than by V5 mapped data. Based on information content for phenomena which vary rapidly in the vertical, V4 mapped temperatures are used in this study.

b. *Rocketsonde data*

Rocketsonde profiles of temperature and wind at LIMS standard pressure levels were obtained in computer tape format from the National Meteorological Data Center. Rocket profiles typically cover the range 50–0.1 mb. Nestler (1983) and Finger et al. (1975) describe the error characteristics of U.S. rocketsonde profiles. The rms differences for paired rocketsondes launched 5 minutes apart are less than 3 K and 10 m s^{-1} below 50 km. Fall rates are very large at low density, being ~200 m s^{-1} near 70 km. Decreased air to wire conduction, aerodynamic heating and lag errors cause temperature data quality to decrease rapidly above 50 km. Typical corrections applied are −2 K at 40 km and −8 K at 60 km. Winds are measured independently from temperature by precision radar tracking of the payload as it descends. Above 50 km, zonal wind profiles provide a more accurate check on LIMS meridional temperature gradients. However, radiosonde tie-on pressure errors, short time-scale atmospheric variability and the discrepancy in sample volume can contribute to LIMS–rocket profile differences.

c. *Wind determination from LIMS*

Geostrophic zonal winds are calculated from fields of geopotential height derived from LIMS thicknesses and National Meteorological Center (NMC) 50 mb height fields which have been Fourier analyzed. Time and longitude variations of tropical deep convective systems can cause sampling biases in LIMS data below 50 mb, so 50 mb tie-on heights are used to prevent upward propagation of these errors. To reduce day to day noise, all 50 mb height coefficients were smoothed once in time with an elemental Gaussian filter having weights ¼, ½, ¼ ("1–2–1 smoothing").

The time variation of the resulting zonal mean tie-on heights at 8°N is shown in Fig. 2. The long-term trend is very similar to the trend in 50 mb temperature reported at Balboa (9°N) by Reed (1962), with minimum values occurring in February. Week-to-week variations that are confined to low latitudes are also seen. In order to suppress propagation of this signal to higher altitudes, each height field was smoothed 1–2–1 in latitude between 16°S and 16°N before building from each level to the next higher level.

The leading terms in the zonal mean meridional momentum equation are $\bar{u}(f+\bar{u}\tan\phi/a) = -\partial\bar{\Phi}/\partial y$, where $\bar{u}$ is the zonal wind, $f = 2\Omega\sin\phi$, ϕ is latitude, a the earth's radius, Ω the angular frequency of the earth's rotation, and Φ the geopotential. If the zonal mean

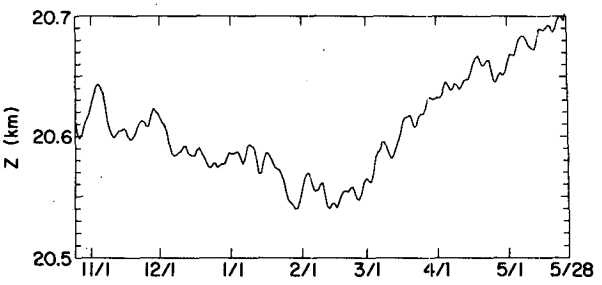

FIG. 2. Time variation of NMC 50-mb zonal mean geopotential height at 8°N.

wind inside the parentheses is approximated by the geostrophic value, $\bar{u}_g = -(1/f)(\partial\bar{\Phi}/\partial y)$, then

$$\bar{u} = \bar{u}_g\left[1+\frac{\bar{u}_g}{2\Omega a\cos\phi}\right]^{-1}. \tag{3.1}$$

A consistent grouping of terms for the perturbation meridional momentum equation gives

$$u' = -\left[f+\frac{2\bar{u}\tan\phi}{a}\right]^{-1}\frac{\partial\Phi'}{\partial y}. \tag{3.2}$$

The perturbation zonal wind is used in this paper to compare longitude-dependent zonal winds derived from LIMS with rocketsonde zonal winds at individual stations. Inclusion of planetary curvature modifies the solution only slightly at low latitudes. Therefore, (3.1) and (3.2) will be referred to as geostrophic winds. Centered differences are used to compute all derivatives. Equatorial values are taken to be the mean of values at 4°S and 4°N. Perturbation zonal winds are smoothed 1–2–1, once in latitude at each level.

Finite differences of $\partial\bar{u}/\partial t$ and $\partial\bar{T}/\partial t$ made from LIMS observations are noisy on a day-to-day basis. Six day averages are used to study acceleration, allowing for an even 36 periods for the 216 day record. These block averages are long enough to provide smooth trends, but week-to-week variations are still captured.

d. *Radiative calculations*

To estimate meridional circulations we require accurate heating rates. The radiative heating code of Wehrbein and Leovy (1982) has been modified by T. Yamasaki and made available to us for this purpose. The code accounts for diurnally varying solar radiation absorption by O_2 and O_3 in the UV and by CO_2 and H_2O in the near-IR. Emission and exchange of IR radiation is calculated using the CO_2 transmission functions of Fels and Schwarzkopf (1981), the O_3 transmission functions of Ramanathan and Dickinson (1979), and the Goody random model modified to allow for Voigt line shape by H_2O. The code employs monthly mean climatological values of tropospheric and mesospheric temperature and ozone fitted

smoothly to the LIMS data, and monthly mean planetary albedo and outgoing longwave radiation. Further details and applications of this model will be described elsewhere (Yamasaki, 1987).

Global mean heating rates in a given layer are expected to be very small. These are estimated by assuming that values from 84° to 68°S are the same as at 64°S, then averaging from 84°S to 84°N, weighting by $\cos\phi$. Each 6-day global average profile of global mean heating is subtracted from each 6-day average heating rate cross section to provide our best estimate of heating rates. Departures of global mean heating from zero are generally much less than 1 K day^{-1}, but they increase above 0.4 mb, reaching almost +3 K day^{-1} at 0.1 mb. These departures are apparently due to some combination of temperature underestimate and ozone overestimate in the LIMS retrievals.

4. Evolution of the zonal mean state

a. *Daily evolution at low latitudes*

The daily evolution of the zonal mean state over the equator is presented in Fig. 3. The altitude scale is the time mean profile of geopotential height. In Fig. 3a the time mean vertical temperature stratification has been removed so that temporal changes are more readily seen. In spite of the approaching equinox, lower stratospheric temperatures reach a minimum in February (Fig. 3a, Fig. 2; Reed, 1962). This suggests that dynamically-driven ascent (cf. Fig. 1a) is particularly strong in February, reaching to 40 km.

In the lower stratosphere QBO easterlies overlie QBO westerlies throughout the LIMS period (Fig. 3b), (Labitzke and Goretzki, 1982). Above 30 km a twice yearly cycle of variation in temperature and zonal wind is suggested in this 7-month data record. Westerlies form near 65 km in late December with maximum westerlies descending to the stratopause by April. The region of maximum westerlies near 40 km in November appears to have descended from about 50 km in October. From November onward easterlies strengthen at each level until the descending westerlies arrive. The lowest layer of westerlies near 35 km disappears just before the beginning of rapid westerly acceleration in the mesosphere.

Both westerly layers overlie shallow warm layers, while easterlies occur in a deep cool layer. A warm/cool pair descends with the primary zero wind line (the line separating easterlies from overlying westerlies and extending from 0.1 mb in December to 7 mb in May). This thermal pattern may be explained by convergent mean vertical motion, which in turn implies the existence of residual mean circulation cells centered about the equator. The warm and cool anomalies are separated by 10–15 km. This pattern evolution results in ranges of 21 K and 105 m s^{-1} in the lower mesosphere (cf. Quiroz and Miller, 1967).

Time mean westerlies are present above 55 km. An asymmetry between the two SAO cycles for this period is also apparent: easterlies appear just above the stratopause in mid-November, but not in mid-May. Belmont et al. (1975) found that during 1961–71 encroachment of easterlies at 50 km into the winter hemisphere was generally more extensive in northern winters. The weaker easterly acceleration in May is insufficient to help shape a well-defined westerly *maximum* which descends with time, such as that seen near 2 mb in November. In contrast, descent of the zero wind line below 5 mb is similar during November and May. The descent rate of the primary zero wind line decreases with decreasing altitude and increasing ambient density. From late December through late April the zero-wind line descends from 65 to 35 km at an average rate of 7 km/mo or 0.3 cm s^{-1}.

Strong week-to-week variations occur. Note the rapid formation of the warm/cool pair and intensification of westerly shear in late December. Another interesting sequence is the cooling and reduction of westerlies in mid-January near 60 km followed by warming and westerly acceleration two weeks later.

Cross-equatorial shear (Fig. 3c) helps determine meridional advection and the likelihood of inertial instability, and so plays a fundamental role in the SAO. In November, $\bar{u}_y$ increases with altitude to 7 day^{-1} at 70 km. Thereafter, the maximum descends with time, lying between the warm/cool pair, at the level of maximum equatorial easterlies. In December the reduction of $\bar{u}_y$ near 0.2 mb coincides with the rapid formation of the warm/cool pair and intensification of westerly vertical shear (Fig. 3b). The most rapid descent of the zero wind line is observed at this time. After 4 April $\bar{u}_y$ reverses and strengthens at all levels.

b. *Structure in latitude–height*

Latitude–height sections of zonal mean temperature and zonal wind depicting structure in November, December, January and May are shown in Figs. 4–7. Also shown are sections of the quantity

$$\tilde{P} \equiv \begin{cases} \dfrac{f}{|f|}\left(\eta - \dfrac{f}{\mathrm{Ri}}\right), & y \neq 0 \\ 0, & y = 0, \end{cases} \tag{4.1}$$

where $\eta = f - \bar{u}_y + \bar{u}\tan\phi/a$ is absolute vorticity, $\mathrm{Ri} = N^2/(\partial\bar{u}/\partial z)^2$ is Richardson number, and N is buoyancy frequency; $\tilde{P}$ has units of vorticity and is closely related to both the zonal mean Ertel potential vorticity and the isentropic gradient of angular momentum per unit mass (cf. section 6). Unless $\bar{u}_y/f > (1 - \mathrm{Ri}^{-1})$, $\tilde{P} \geqslant 0$. This exceptional condition is the necessary condition for inviscid inertial instability, and it will be referred to in the following as anomalous $\tilde{P}$.

By early November a westerly jet is already well-established near 50°N, 0.3 mb, with a subtropical me-

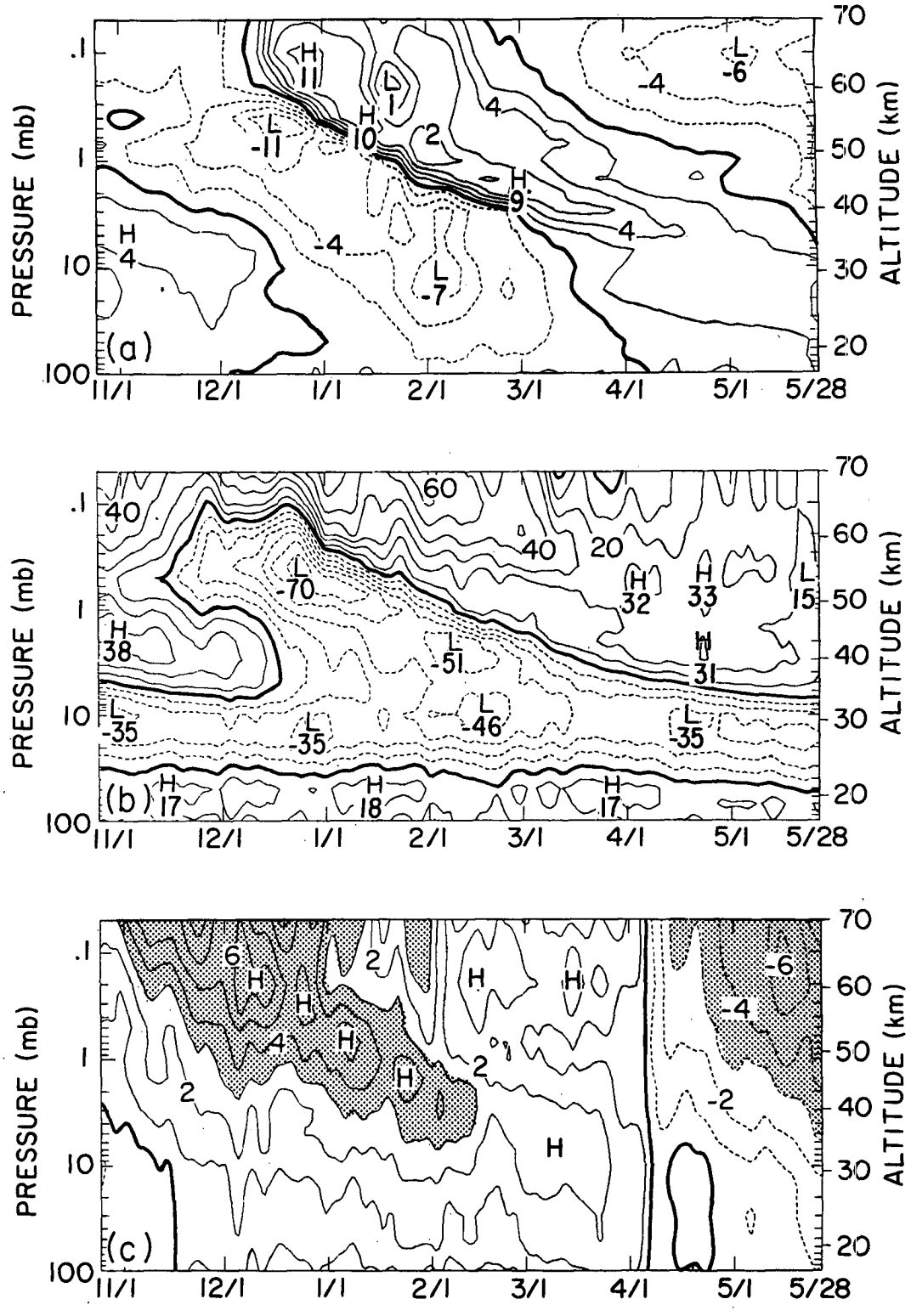

FIG. 3. Time–height sections of LIMS zonal mean (a) temperature, (b) zonal wind and (c) northward shear of zonal wind, with contour intervals 2 K, 10 m s^{-1} and 1.0 day^{-1}, averaged in the latitude band 8°S–8°N. In (a) the time mean profile has been subtracted out. In c, values exceeding ±3 day^{-1} are shaded. The values have been smoothed 1–2–1 in time.

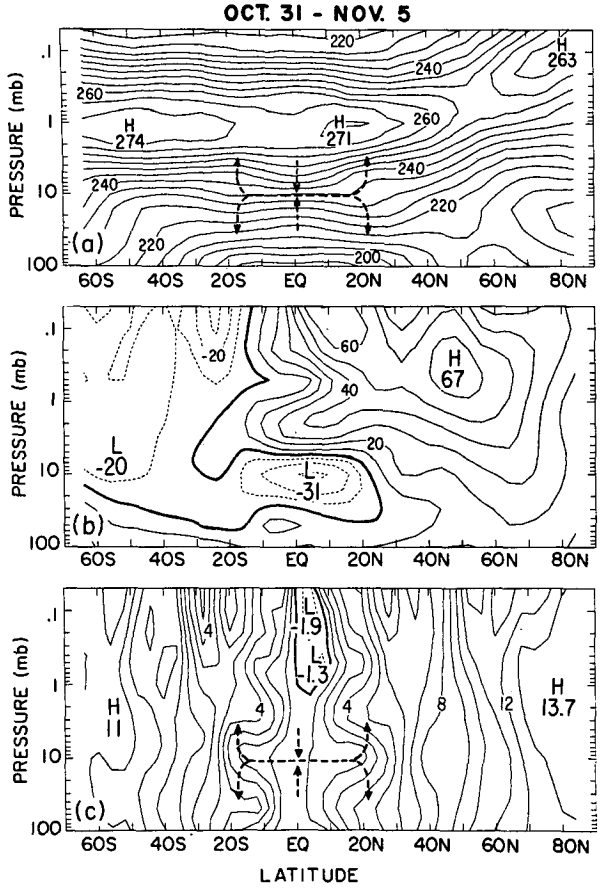

FIG. 4. Latitude–height sections of zonal mean LIMS (a) temperature, (b) zonal wind and (c) the quantity (4.1), an indicator of anomalous angular momentum gradient for the period 31 October–5 November 1978, with contour intervals 5 K, 10 m s^{-1} and 1.0 day^{-1}. Values of temperature and zonal wind have been smoothed 1–2–1 in latitude. The schematic arrows indicate possible meridional circulations which could account for the observed temperature pattern.

sospheric jet near 10°N, 0.05 mb (Fig. 4b). The summer hemisphere easterly jet near 25°S, 0.05 mb is not yet well developed. A lobe of SAO westerlies is centered over the equator near 2 mb, overlying a core of QBO easterlies. In the equatorial mesosphere meridional temperature gradients are weak (Fig. 4a) and cross-equatorial shears are moderately strong. The value of $\tilde{P}$ is anomalous in the winter mesosphere equatorward of ~10°N (Fig. 4c).

An interesting temperature pattern exists in the region 30°S–30°N, 30–3 mb. Below 10 mb, isotherms are deformed upward over the equator and downward in the subtropics, with the opposite pattern above 10 mb. This structure is verified by rocket profiles at Kwajalein (8.7°N) and Barking Sands (22°N) (not shown). The schematic arrows in Fig. 4a suggest mean meridional circulations which could account for this temperature pattern. Downward motion is inferred in the westerly shear, with meridional divergence near the level of maximum easterlies. This inferred circulation appears to have advected low values of $\tilde{P}$ poleward near 10 mb (Fig. 4c).

From early November to mid-December very strong changes are observed in the mesosphere. Above 0.4 mb equatorial temperatures are now considerably higher than subtropical temperatures (Fig. 5a). The easterly jet near 25°S has strengthened greatly, with large values occurring very close to the equator near 0.4 mb. Although the equator appears to act as a barrier to these easterlies, the zero wind line has moved from 10°S as far as 16°N during this time. The low latitude mesospheric westerly wind maximum at 0.05 mb is now near 4°N. Above 0.4 mb westerly vertical shear has greatly increased, while meridional shears in the latitude band 4°–12°N have decreased (compare Figs. 4b, 5b), in opposition to the seasonal trend of thermal wind expected from radiative forcing approaching the solstice. The region of anomalous $\tilde{P}$ near 4°N has descended and two secondary regions have developed near 8°S and 20°N at 0.4 mb (Fig. 5c). The details of the $\tilde{P}$ distribution very close to the equator may not be precisely depicted by these data, but it is clear that

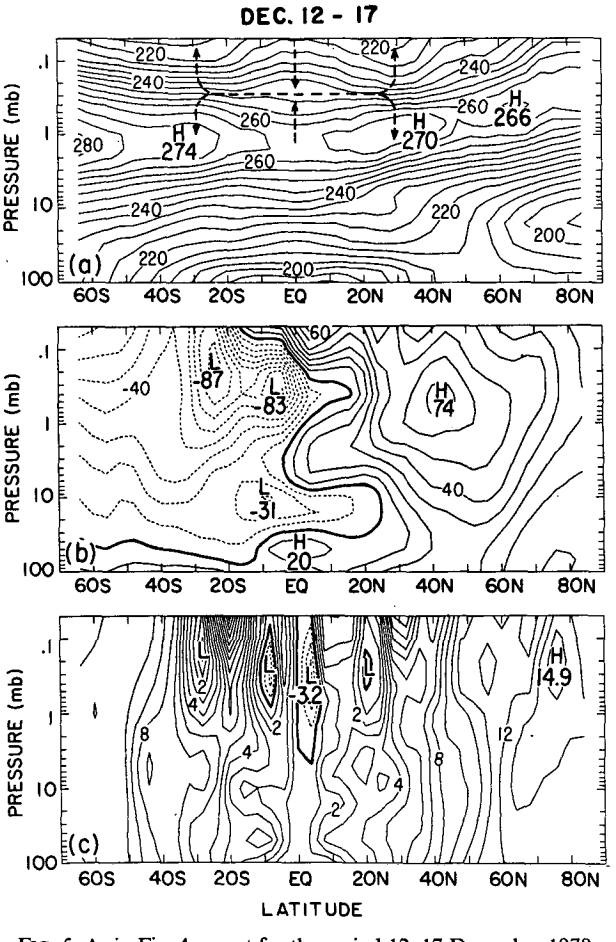

FIG. 5. As in Fig. 4 except for the period 12–17 December 1978.

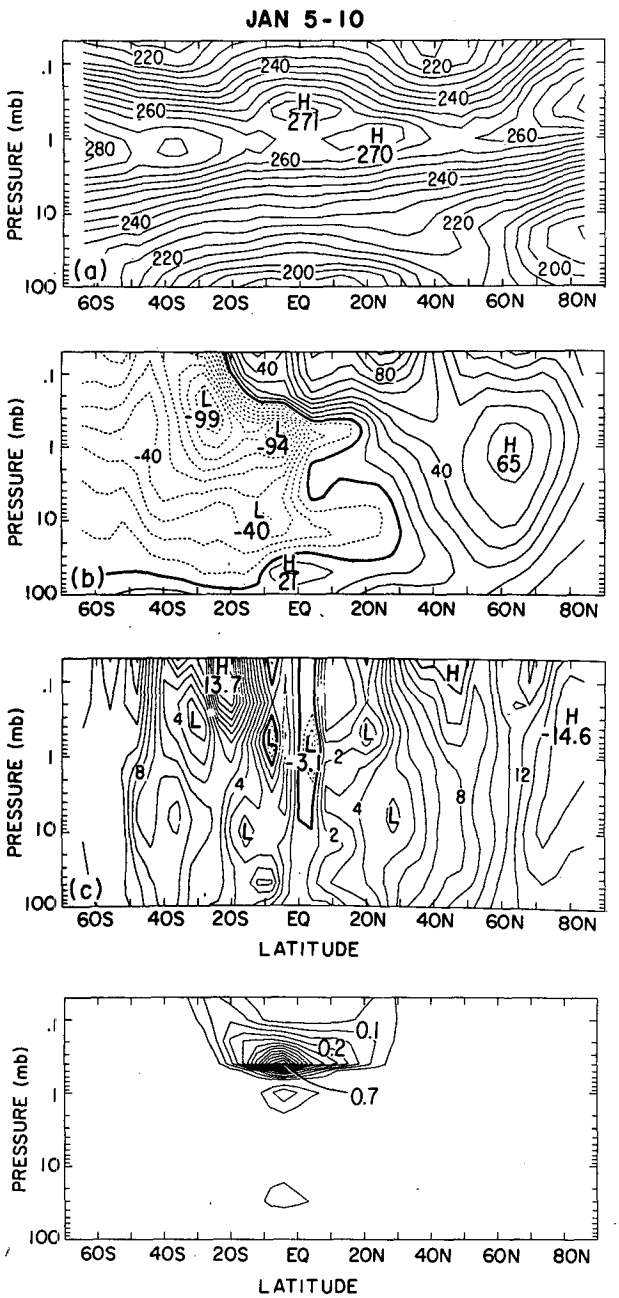

FIG. 6. As in Fig. 4 except for the period 5–10 January 1979. Values of Ri^{-1} are contoured in the lower panel, with interval 0.05.

low or even anomalous values of $\tilde{P}$ extend poleward to beyond 20°N and 10°S near the 0.3 mb level.

The meridional circulation inferred from the temperature distribution in mid-December (Fig. 5a) gives descent in the westerly shear zone and divergent meridional flow at the level of maximum easterlies near 0.4 mb. A dramatic redistribution of angular momentum in the equatorial mesosphere appears to be associated with amplification of SAO meridional circulations in mid-December (cf. Fig. 3).

During the next three weeks further strong changes in the latitudinal temperature structure occur in the mesosphere (Fig. 6a). Above 0.4 mb latitudinal variation increases and the temperature minima shift poleward. In the layer 0.7–0.4 mb subtropical temperature gradients reverse (compare Fig. 5a). A double stratopause structure exists near the equator. SAO westerlies have begun to descend and the easterlies below have intensified further (Fig. 6b). The winter westerly jet has moved poleward and downward, while the zero-wind line has advanced poleward over the deep layer 30–0.4 mb. The weak meridional shear evident near 0.5 mb, 10°N (Fig. 6b) has been verified by comparing rocket profiles at Antigua (17°N) and Kwajalein (8.7°N). Easterlies have reached Antigua (17°N) near 0.5 mb (not shown). During the northern midwinter it is common for lower mesospheric easterlies to reach ~20°N, and in some years as far as 30°N (Belmont et al., 1975).

The regions of anomalous $\tilde{P}$ have descended with the zero-wind line and are smaller in magnitude than they were in December (Figs. 5c, 6c). In fact, by late January, the secondary regions have disappeared, co-

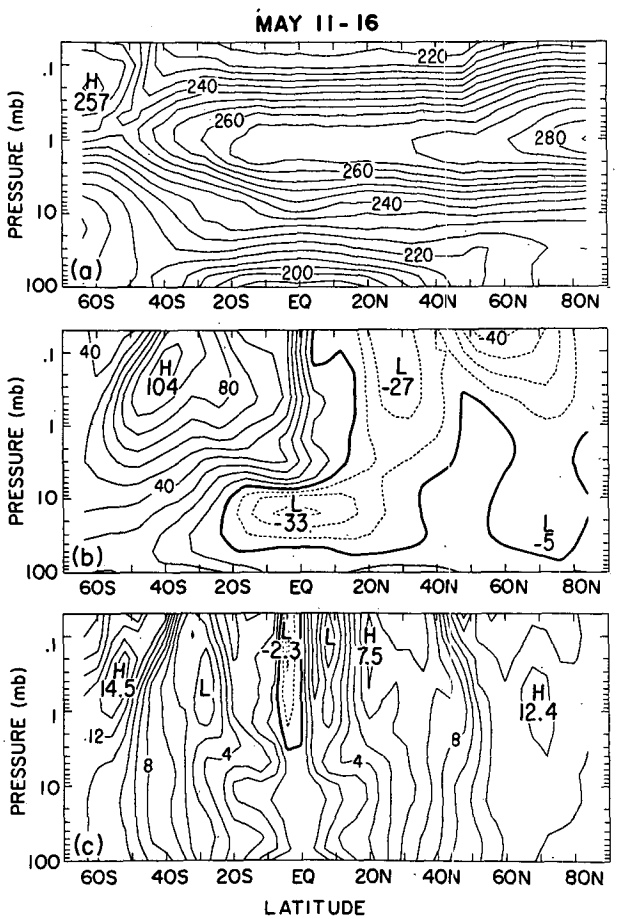

FIG. 7. As in Fig. 4 except for the period 11–16 May 1979.

inciding with the disappearance of the SAO westerlies near 3 mb (not shown).

By May the equatorial SAO warm anomaly has reached 7 mb (Fig. 7a), with inferred circulation cells similar to those in November. Once again, strong westerlies have formed in the winter hemisphere well before strong easterlies in the summer hemisphere. The rather uniform strong cross-equatorial shear above 7 mb is unaccompanied by any noteworthy vertical shear (Fig. 7b). The region of anomalous $\tilde{P}$ is again located in the winter hemisphere and is restricted to a narrow latitude band.

c. *Validation*

Time series of 6-day average binned rocket profiles and LIMS profiles of zonal wind, obtained by linear latitudinal interpolation and longitudinal expansion of coefficients to station locations, are compared in Fig. 8. The mean time between rocket profiles is 2.8 days. Bins with no rocket data are left blank.

Figure 8 illustrates how well LIMS captures the location and magnitude of intense vertical shear. Although ranges in LIMS geostrophic winds are 10%–25% larger than for rocket winds, the relatively good agreement supports the use of geostrophic winds for large-scale phenomena, even near the equator.

The rocket LIMS comparison in Fig. 9 for early January illustrates the typical scatter in rocket profiles during a 12-day period. At Ascension Island and Kwajalein rocket profiles also exhibit a double stratospause, an easterly jet near 0.7 mb, and very strong westerly vertical shear above that level. The asymmetry between 8°S and 9°N in the descending westerlies near 0.4 mb is also evident (Fig. 6b). Cross-equatorial shears of ~ 3 day^{-1} near 1 mb are substantiated (Fig. 3c).

Wind shear agreement implies that horizontal temperature gradients are well represented by LIMS. Rocket values at 0.4 mb (Fig. 10) validate the large variation of temperature with latitude seen by LIMS in early January (Fig. 6a).

d. *Relationship between tropics and extratropics*

An overview of latitudinal relationships is afforded by examining latitude–time sections at selected levels. In Fig. 11 the equatorial SAO warm layer begins to form near 0.2 mb in early December, but does not

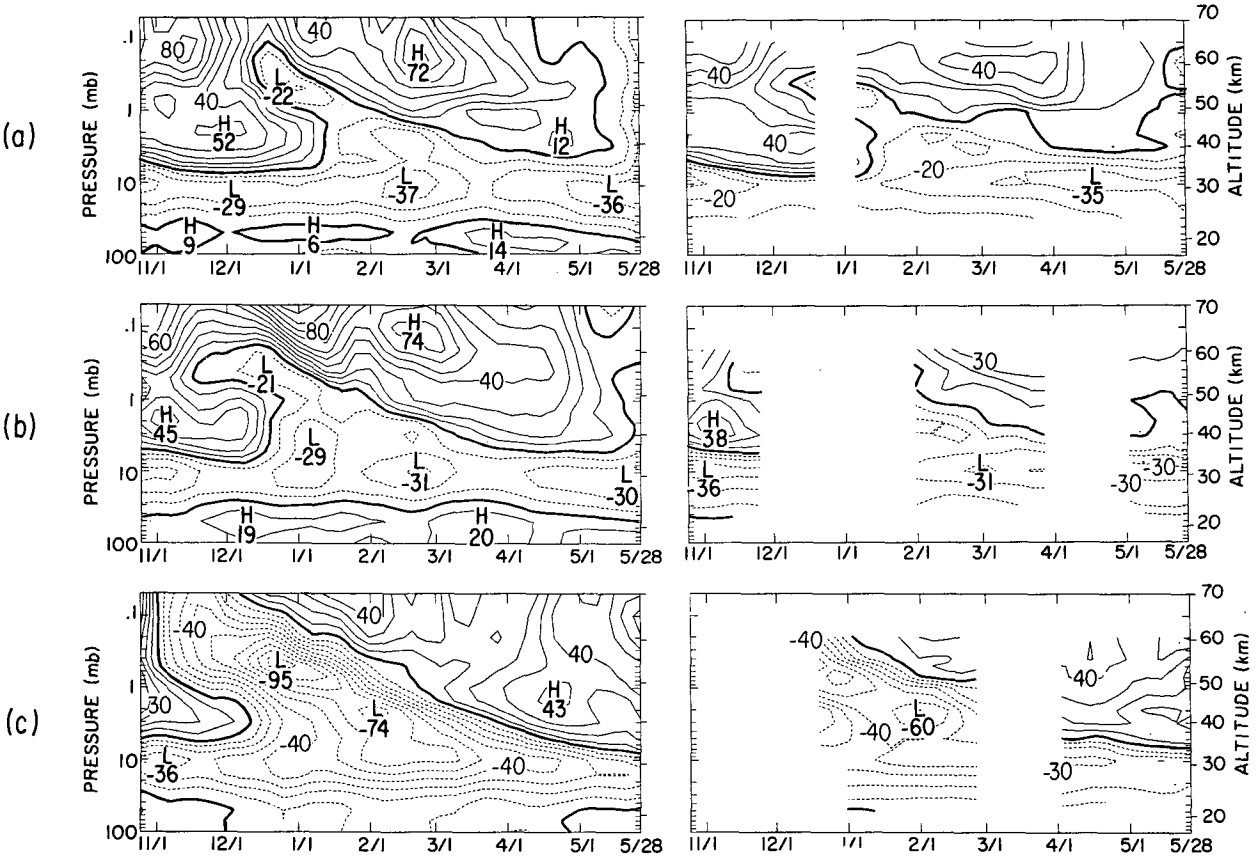

FIG. 8. Time–height sections of rocket (right) and LIMS (left) profiles of zonal wind at (a) Kwajalein (8.7°N, 167.7°E), (b) Fort Sherman (9.3°N, 80.0°W) and (c) Ascension Island (8.0°S, 14.5°W), contour interval 10 m s^{-1}.

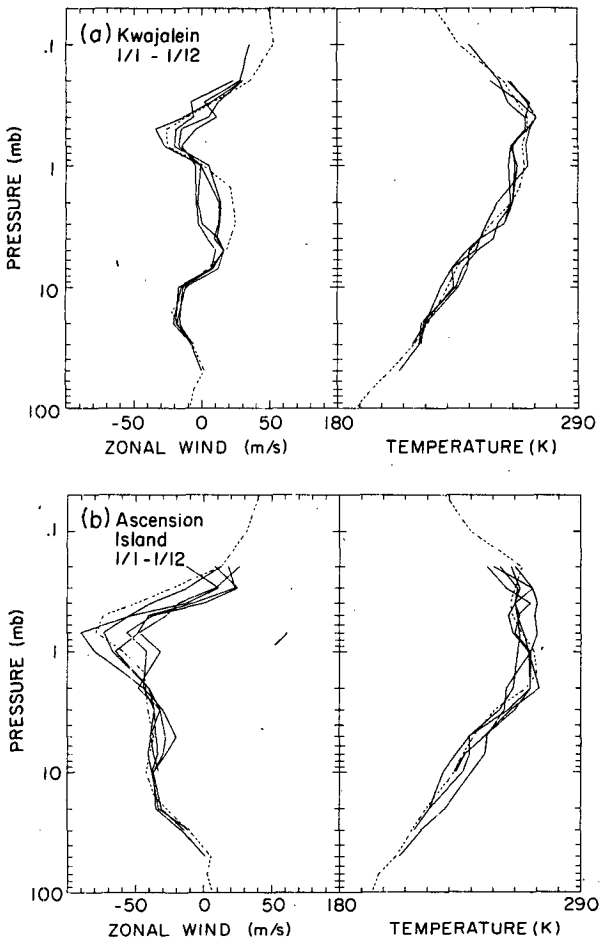

FIG. 9. A comparison of all rocket soundings (solid) and the LIMS time average profiles (dashed) of zonal wind and temperature for the period 1–12 January 1979 at (a) Kwajalein (8.7°N, 167.7°E), (b) Ascension Island (8.0°S, 14.4°W).

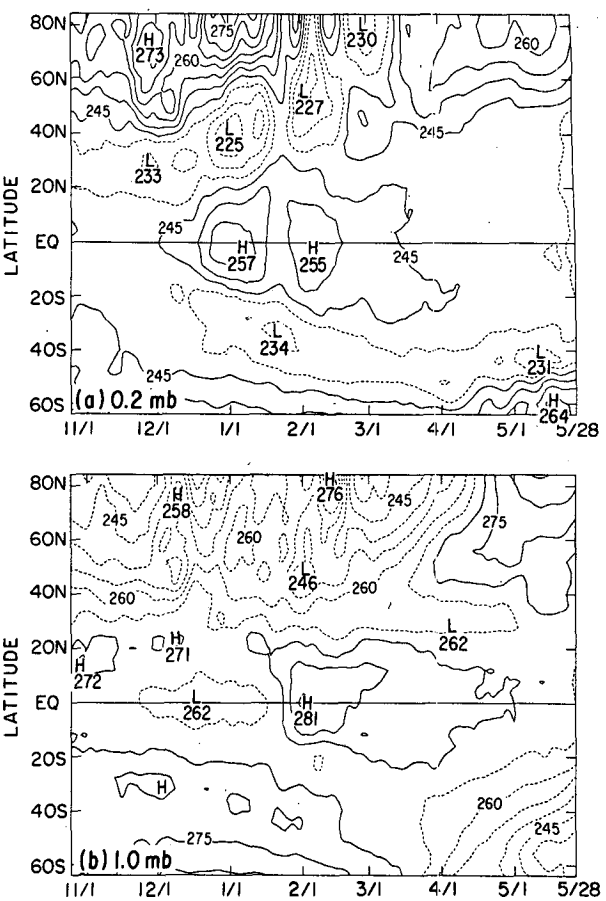

FIG. 11. Latitude–time section of LIMS zonal mean temperature at (a) 0.2 mb and (b) 1.0 mb. The contour interval is 5 K. Contours are dashed for temperatures below 245 K in (a) and below 270 K in (b). The values have been smoothed 1–2–1 in time.

reach 1.0 mb until late January (cf. Fig. 3a). The SAO cold layer passes through the 1.0 mb level from late November through early January. As the equatorial warm anomaly at 0.2 mb amplifies and spreads in latitude, flanking cold anomalies also amplify and migrate poleward, with larger amplitudes in the winter hemisphere. Amplitude variations near 0° and 40°N are correlated in time. Relative maxima on the equator correlated with midlatitude minima occur near 1 January at 0.2 mb and near 1 February at both levels.

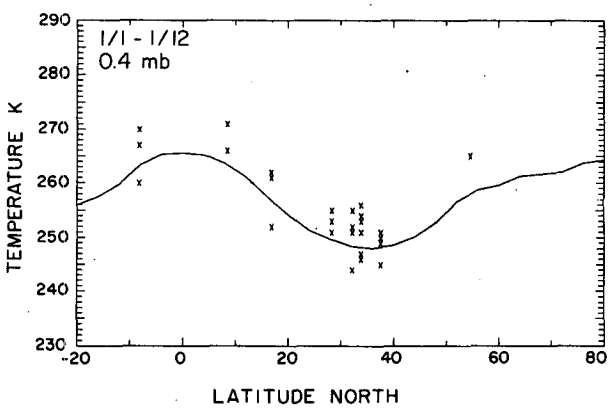

FIG. 10. Temperatures at 0.4 mb seen by western hemisphere rockets (crosses) and by LIMS (solid line), averaged over the longitude band 60°–180°W for the period 1–12 January 1979.

This simultaneity is further evidence that these temperature anomalies are manifestations of large-scale meridional circulations that are spun up on the time scale of wave driving. By comparing Figs. 12a and 3a it can be seen that near 1 February the inferred circulation near the stratopause is similar to Fig. 1a: vertical divergence at high latitudes, convergence over the equator, and poleward motion at midlatitudes. Rossby wave driving in the winter hemisphere can induce a polar stratospheric warming and amplify vertical motions over the equator.

To contrast and compare the equatorial and high latitude SAO, time–height sections of temperature at 60°–64°N and 64°–60°S are shown in Figs. 12b, c.

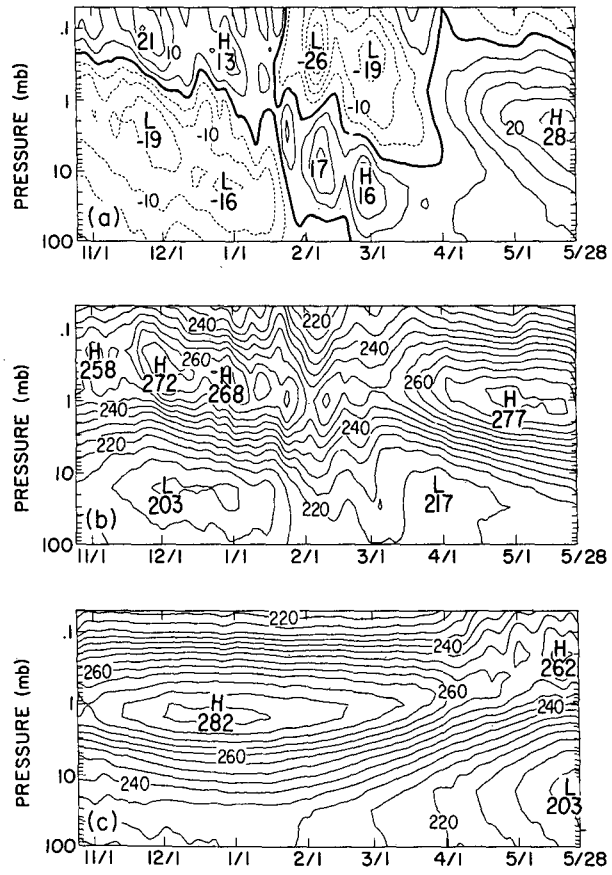

FIG. 12. Time–height sections of LIMS zonal mean temperature averaged over the latitude band (a) 64°–72°N, (b) 60°–64°N, and (c) 64°–60°S. The contour interval is 5 K. In (a) the time mean profile has been removed. Values have been smoothed 1–2–1 in time.

During the overlapping transitional periods, 24 April–28 May and 25 October–28 November, temperature values and trends are quite similar in the two hemispheres. Figures 12b, c may be regarded as a rough estimate of a full year's variation in either hemisphere. Mesospheric cooling and stratospheric warming can be described as a lowering of the stratopause altitude. The stratopause altitude reaches a smooth minimum near the summer solstice (Fig. 12c) and is highest in early winter (late November, Fig. 12b; late May, Fig. 12c). During winter there is an irregular downward trend varying on the time scale of wave driving. This trend is an accumulation of individual short events which interrupts the smooth annual cycle and imparts a semiannual component to the variation. These events appear to be distributed globally through meridional circulations such as those in Fig. 1a.

At 0.5 mb the westerly jet near 40°N begins to migrate poleward as easterlies penetrate across the equator in mid-December (Fig. 13a). In fact, from mid-December to early February the westerly jet steadily moves poleward and downward (Figs. 5b, 6b, 13a, b) as the zero wind line migrates northward and the equatorial stratosphere cools (Fig. 3a). At 7 mb (Fig. 13b) the zero wind line advances all the way to 45°N by February, followed by the well-known flow reversal at high latitudes.

5. Advection by mean meridional circulations

a. Estimation of the residual mean circulation

In this section the inferred mean meridional circulations and their effects are described quantitatively, based on calculations for successive 6-day mean temperature and ozone cross sections. The transformed Eulerian zonal mean primitive equations in log-pressure coordinates are (Dunkerton et al., 1981)

$$\frac{\partial \bar{u}}{\partial t} - \eta \bar{v}^* + \bar{w}^* \frac{\partial \bar{u}}{\partial z} = \bar{F} + \mathrm{DF} \qquad (5.1)$$

$$\left(f + \frac{2\bar{u}\tan\phi}{a}\right)\frac{\partial \bar{u}}{\partial z} + \frac{g}{\theta_0}\frac{\partial \bar{\theta}}{\partial y} \approx 0 \qquad (5.2)$$

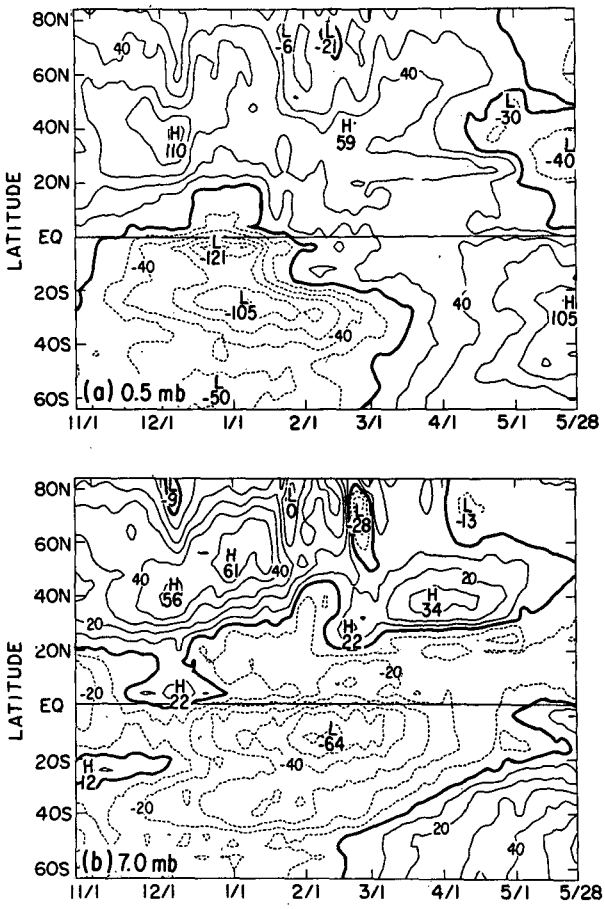

FIG. 13. Latitude–time sections of LIMS zonal mean zonal wind at (a) 0.5 mb, contour interval 20 m s^{-1} and (b) 7.0 mb, contour interval 10 m s^{-1}. Values have been smoothed 1–2–1 in time.

$$\frac{1}{\cos\phi}\frac{\partial}{\partial y}(\bar{v}^*\cos\phi)+\frac{1}{\rho_0}\frac{\partial}{\partial z}(\rho_0\bar{w}^*)=0 \quad (5.3)$$

$$\frac{\partial\bar{\theta}}{\partial t}+\bar{v}^*\frac{\partial\bar{\theta}}{\partial y}+\bar{w}^*\frac{\partial\bar{\theta}}{\partial z}=\bar{Q}+\mathrm{DQ}. \quad (5.4)$$

Here $\bar{\theta}$, $\bar{F}$, $\bar{Q}$ are the zonal mean potential temperature, mechanical dissipation due to small scale eddies and diabatic heating; θ_0 and ρ_0 are the global mean profiles of potential temperature and density; $\bar{v}^*$ and $\bar{w}^*$ are the components of the residual mean circulation, which corresponds approximately to the actual material transport and is nonzero only if there are nonconservative processes: diabatic heating, wave transience or dissipation (Andrews and McIntyre, 1976; Boyd, 1976; Edmon et al., 1980). The full representation of the terms DF and DQ due to large-scale eddies is given in Appendix A of Dunkerton et al. Wave temperatures were used to estimate DQ. For most situations it was found to be much smaller than the remaining terms. To a good approximation (5.4) may be rewritten

$$\frac{\partial\bar{T}}{\partial t}+\bar{v}^*\frac{\partial\bar{T}}{\partial y}+\frac{\bar{T}N^2}{g}\bar{w}^*=\bar{J}, \quad (5.5)$$

where $\bar{J}$ is the radiative heating rate and g is gravitational acceleration.

Equations (5.1)–(5.4) may be combined into a single equation for meridional streamfunction which, from scale analysis, reduces to

$$\frac{\partial}{\partial y}\left(\frac{\chi_y}{\cos\phi}\right)=\frac{g\rho_0}{\bar{T}N^2}\frac{\partial\bar{J}}{\partial y} \quad (5.6)$$

at low latitudes (Meyer, 1970; Plumb and Bell, 1982), where

$$\chi_y=\rho_0\cos\phi\bar{w}^*;\quad \chi_z=-\rho_0\cos\phi\bar{v}^*. \quad (5.7)$$

To obtain a first-guess residual circulation, (5.6) is solved by the tridiagonal method with the assumption of zero meridional motion at 64°S and 84°N. Using this solution as the first guess for $\bar{v}^*$, a more accurate estimate of the residual circulation is obtained by iterating (5.5) and (5.3). First, $\partial\bar{T}/\partial y$ is smoothed 1–2–1 in latitude. Then (5.5) is solved for $\bar{w}^*$ using the first guess for $\bar{v}^*$. The global mean profile of $\bar{w}^*$ is then subtracted, (a very small correction), and (5.3) is solved for a new estimate of $\bar{v}^*$. In solving (5.3), $\bar{v}^*=0$ at 84°N, but is allowed to be nonzero at 64°S. Then $\bar{v}^*$ is smoothed 1–2–1 in latitude and (5.5) is solved for $\bar{w}^*$ again. This procedure is repeated five times. Excellent convergence is obtained, with rms differences between successive fields of $\bar{w}^*$ being very small after the second iteration.

Deduced equatorial profiles of $\bar{J}$, $\bar{w}^*$ and $\bar{v}^*$ are shown in Fig. 14. In (5.5) over the equator subsidence warming is balanced primarily by radiative cooling, except at the base of the warm anomaly where the time derivative in (5.5) is significant. Over the equator,

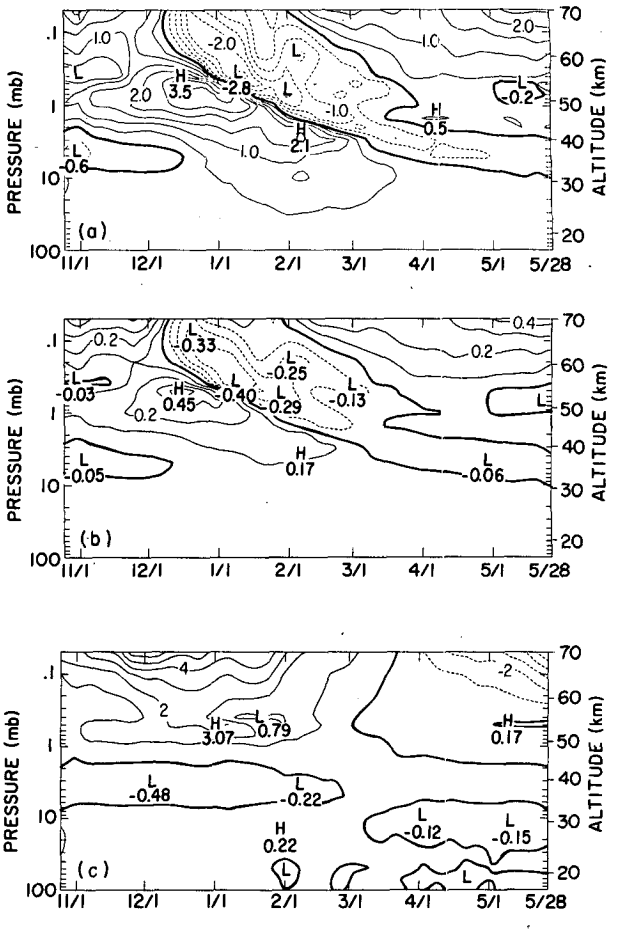

FIG. 14. As in Fig. 3 except of (a) radiative heating rate, contour interval 0.5 K day^{-1}, (b) vertical and (c) meridional components of the residual circulation obtained by iterating (5.3) and (5.5), (see text), contour intervals 0.1 cm s^{-1} and 1 m s^{-1}. Six-day averages are used.

the time and vertical mean of the ratio $|\partial\bar{T}/\partial t|/|\bar{J}|$, calculated on a point-by-point basis, is 0.31. Meridional advection, $\bar{v}^*\bar{T}_y$, also plays a role in the mesosphere. The effect of including it is to shift the $\bar{w}^*$ pattern southward and enhance $\bar{w}^*$ in the region of ascent in the northern subtropics by a factor of ~2. The 11 and −11 K mesospheric anomalies in December (Fig. 3a) are maintained by $\bar{w}^*\sim-0.31$ cm s^{-1} and ~ 0.45 cm s^{-1} (Fig. 14b). The −7 K anomaly near 10 mb in early February requires only $\bar{w}^*\sim 0.08$ cm s^{-1}, due to the longer radiative decay time scale and increased static stability of the stratosphere. Bands of cooling in Fig. 14a are centered on the descending SAO zero-wind lines (Fig. 3b). Note that calculated descent velocities are comparable to the rate of descent of the zero wind lines (Fig. 14b).

In the mesosphere, cross-equatorial flow is from the summer to winter hemisphere, the flow reversing in March (Fig. 14c). A local maximum in $\bar{v}^*$ occurs at the level of vertical convergence (Fig. 14b) which de-

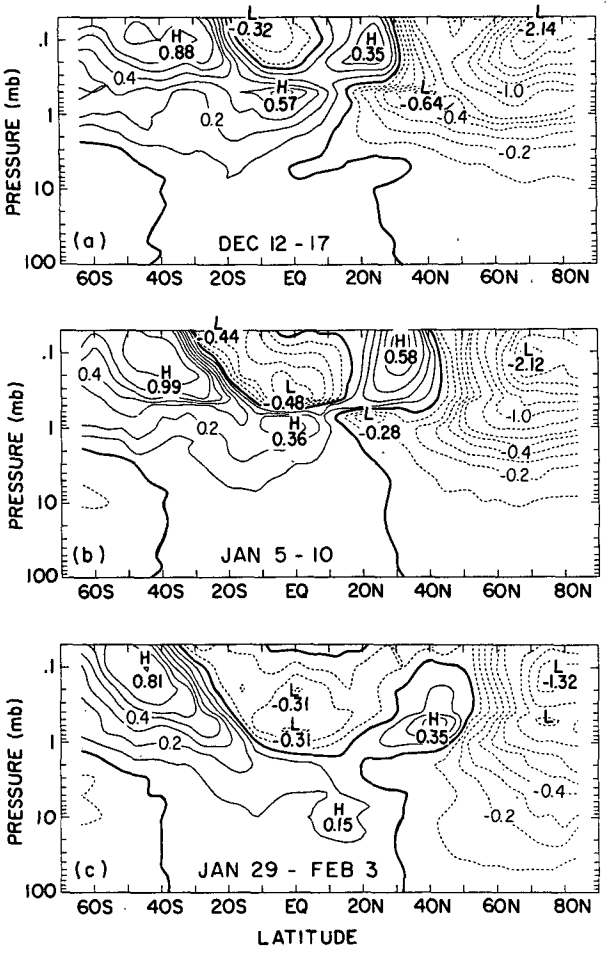

FIG. 15. Vertical component of residual circulation for the periods (a) 12–17 December 1978, (b) 5–10 January 1979 and (c) 29 January–3 February 1979. The contour interval is 0.1 cm s^{-1}.

scends during December–January. The structure of the deduced residual mean circulation in the meridional plane is illustrated in Figs. 15 and 16.

Superimposed on the basic mesospheric pattern of summer ascent in a cold region and winter descent in a warm region is a pattern which is nearly symmetric about the equator, where vertical convergence over the equator pairs with vertical divergence in midlatitudes (Fig. 15). As this equatorially symmetric residual mean vertical velocity pattern descends from mid-December through early February, its latitudinal scale expands from ~30° to ~45° (cf. Fig. 11a). In early January a jetlike maximum of $\bar{v}^*$ extends from ~10°S to ~50°N near 0.5 mb, reaching a maximum speed of ~5 m s^{-1} near 16°N (Fig. 16). Interhemispheric flow is concentrated between the warm/cool pair at the level of maximum $\bar{u}_y$ (Fig. 3c) and level of minimum $\tilde{P}$, enabling advection of easterlies across the equator where $\tilde{P}$ is anomalous (Fig. 6b, c).

The equatorially symmetric part of the calculated residual mean circulation is quite similar to that anticipated from the temperature distribution (Figs. 5a, 15a). In the lower mesosphere near 40°N, this circulation may contribute to the poleward and downward displacement of the main westerly jet (Figs. 5b, 6b, 13a). Near 40°N, 7 mb in Figs. 16 and 17, $\bar{v}^* \sim 0.6$ m $s^{-1} \sim 0.5°$ day^{-1}, a rate that is similar to the poleward advance of the jet maximum in Fig. 13b. Potential vorticity has been used as an indicator of the shape of the polar vortex (McIntyre and Palmer, 1983). The rate of northward shift in locations of the 8 and 12 contours of $\tilde{P}$ near 50°N from mid-December to early January (Figs. 5c, 6c) is similar to $\bar{v}^*$. It is likely that meridional potential vorticity advection contributes to shrinking of the polar vortex.

Figure 17 shows the residual (nearly the Lagrangian) mean meridional circulation near 1 February in vector form. The stratospheric mass flow is similar to that found by Murgatroyd and Singleton (1961), with ascent over the equator and descent at high latitudes. The descending SAO pattern that includes descent over the equator and rising motion in the subtropics near 0.5 mb in Fig. 17 will modify the distributions of water vapor (Remsberg et al., 1984b, Gordley et al., 1985), and methane and nitrous oxide (Solomon et al., 1986, Gray and Pyle, 1986).

Equatorial time–height sections of observed acceleration, vertical advection, and the sum of terms on the lhs of (5.1) are shown in Fig. 18. In December easterly accelerations of ~1.0 m s^{-1} per day occur over a deep layer centered near the stratopause (Fig. 18a). Westerly accelerations are typically stronger (2.0 m s^{-1} per day) and occur in shallow layers that descend with time. As a consequence of the fact that $\bar{w}^* \sim -\delta\bar{T}$ and the thermal wind law, $\bar{u}_z \sim -\bar{T}_y \propto \delta\bar{T}$, acceleration of the zonal flow by vertical advection, $-\bar{w}^*\bar{u}_z \propto (\delta\bar{T})^2$, is predominantly in the westerly sense (Fig. 18b). Much of the observed westerly acceleration can be explained by downward advection in SAO westerly shear layers. Shapes and, to a lesser extent, magnitudes are quite similar in Figs. 18a, b. Figure 18b even picks up the secondary region of westerly acceleration beginning near 0.1 mb in late January, and descending above the main band of westerly acceleration. However, the ef-

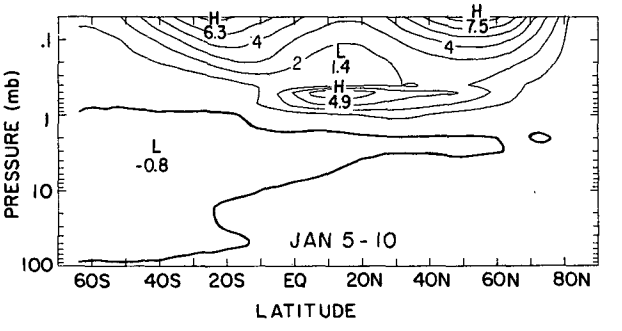

FIG. 16. Meridional component of residual circulation for the period 5–10 January 1979. The contour interval is 1 m s^{-1}.

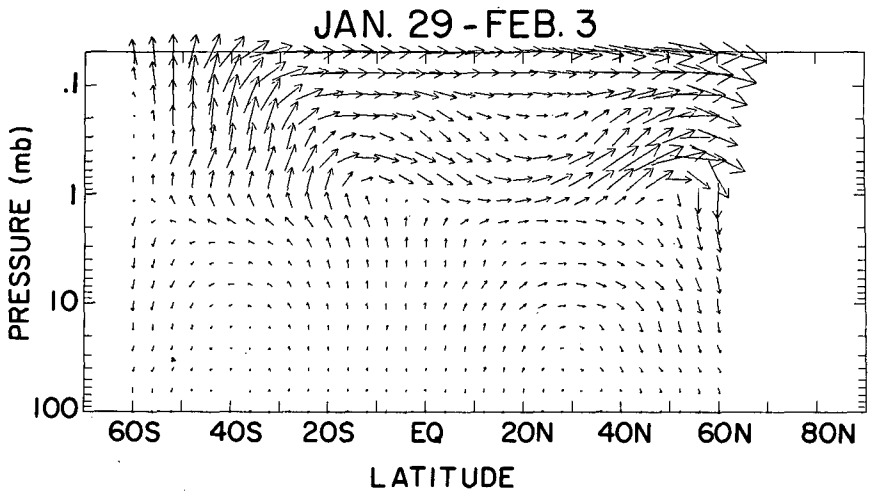

FIG. 17. Residual circulation for the period 29 January–3 February 1979. $\bar{w}^*$ is multiplied by 450 relative to $\bar{v}^*$ prior to plotting.

fects of vertical advection are more than offset by those of meridional advection (Fig. 18c). During November–February northward mesospheric flow (Fig. 14c) advects easterly angular momentum across the equator, so that the lhs of (5.1) is largely positive in this region.

The residual (Fig. 18c) shows the distribution of the body force per unit mass due to eddies of all scales which is required to complete the momentum budget over the equator. Calculations of DF due to LIMS-observed Kelvin and Rossby waves can partially account for the required westerly and easterly wave driving. It is apparent, however, that some other mechanism must also be operating. The correlation of positive and negative regions in Fig. 18c with regions of positive and negative vertical shear in Fig. 3b suggests that absorption of gravity waves is probably important. These results will be described more extensively in a future paper.

b. A possible explanation for the "nose"

A peculiar aspect of the SAO westerlies at 7 mb during December and May is their narrow latitudinal scale (Fig. 13b). Even with the limited latitudinal resolution of the LIMS data, a "nose" clearly seems to be characteristic of the leading edge of the descending SAO westerlies in the stratosphere. This is similar to the feature discussed by Hamilton (1984) and Dunkerton and Delisi (1985) for the QBO. Moreover, the latitude of maximum values is shifted to 4°N during the northern winter and to 4°S during the southern winter. The narrow scale and skewing of the westerly maximum toward the winter hemisphere can also be seen near 7 mb in Figs. 5b, 6b and 7b.

At the level of maximum wave driving near "DF" in Fig. 1b, $\bar{w}^* \sim 0$. Ignoring vertical advection and mechanical dissipation at this level, the latitudinal profile of zonal flow acceleration for a wave driving event may be estimated from (5.1): $\partial\bar{u}/\partial t \sim \mathrm{DF} + \eta\bar{v}^*$. To fix ideas, specific shapes are assumed for $\bar{v}^*$, DF and $\bar{u}_y$. The assumed shape for $\bar{v}^*$ is $\bar{v}^* = v_0 \times \sin(5.7y)$ where $v_0 = -1$ m s^{-1} and y is in degrees latitude. Maximum equatorward motion occurs near 16°, with the cells extending to 32° (e.g., near 3 mb in Fig. 4). The shape for DF is $\mathrm{DF} = \mathrm{DF}_0 \exp[-(y/L)^2]$ where $\mathrm{DF}_0 = 4.0 \times 10^{-5}$ m-s^{-2} and $L = 17°$, since a typical quarter-power latitude for Kelvin waves is 20° (Salby et al., 1984). We assume that $\bar{u}_y = \Gamma = 2.0$ day^{-1} (Fig. 3c).

Without any residual circulation, the latitudinal profile of $\partial\bar{u}/\partial t$ should have the same shape as the curve DF in Fig. 19a. When this wave driving event occurs in the presence of previously established circulation cells but no meridional wind shear, Coriolis torques will effectively narrow the latitudinal scale of zonal flow acceleration, as suggested by the dashed curve in Fig. 19a. In the presence of meridional shear the peak is shifted into the winter hemisphere (Fig. 19b).

While this problem really should be treated in a numerical model, allowing for a latitudinal dependence of $\bar{u}_y$, this simple analysis suggests that when background SAO or QBO westerlies experience accelerations such as those shown in Fig. 19, a local wind maximum can form. When this maximum is advected downward, the first westerlies to arrive will be in a narrow band. If this interpretation is valid, the nose seen in descending equatorial westerlies can be explained by the modification of a wave driving event by the extant residual circulation.

6. The possible role of inertial instability

The inertial stability of a region depends on the sign of the potential vorticity, or equivalently, of the angular

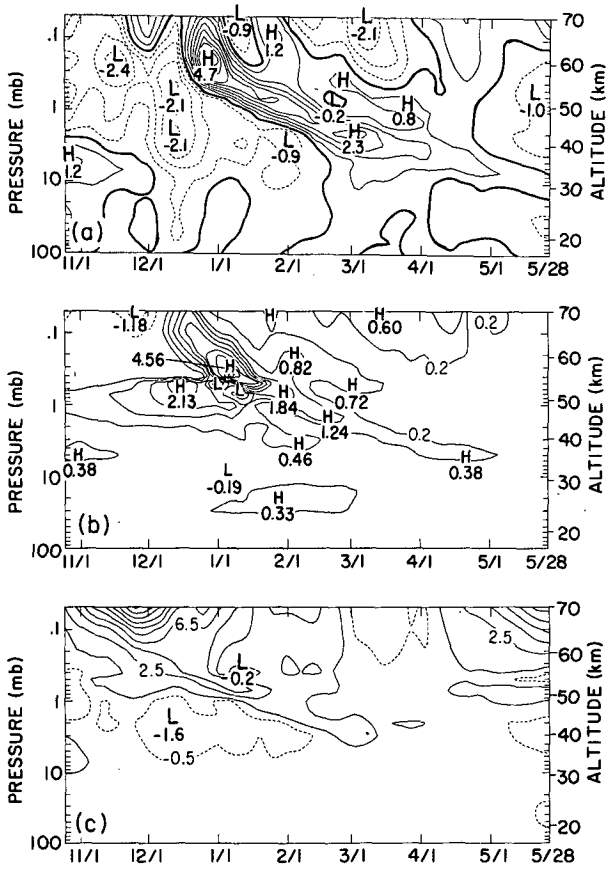

FIG. 18. As in Fig. 14, except of (a) observed acceleration of zonal mean zonal wind, contour interval 0.5 m s^{-1} per day, (b) vertical advection, $-\bar{w}^*\bar{u}_z$ and (c) the sum: $\bar{u}_t + \bar{w}^*\bar{u}_z - \eta\bar{v}^*$. In (b) and (c) the zero contour is omitted for clarity. In (b) contours begin at ±0.2, with interval 0.5 m s^{-1} per day. In (c) they begin at ±0.5, with interval 2.0 m s^{-1} per day.

momentum gradient. The criterion for inviscid symmetric inertial instability is

$$f(\eta - f/\mathrm{Ri}) < 0 \tag{6.1}$$

(Eliassen and Kleinschmidt, 1957).

The zonal mean Ertel potential vorticity is

$$\bar{P} = \frac{\bar{\theta}_z}{\rho_0}(\eta - f/\mathrm{Ri}) \tag{6.2}$$

(Hoskins et al., 1986). In the absence of shear $\bar{P}$ increases monotonically from the South Pole to the North Pole, is zero at the equator, and $f\bar{P} \geqslant 0$ everywhere. The northward gradient of angular momentum, $M = r\bar{u} + r^2\Omega$, along an isentropic surface is

$$\nabla_\theta M = -r\left(\eta - \frac{f}{\mathrm{Ri}}\right), \tag{6.3}$$

where $r = a\cos\phi$. In (6.3) it is assumed that the thermal wind law is valid. In the absence of shear M is largest at the equator, and $f\nabla_\theta M \leqslant 0$ everywhere. From (6.2) and (6.3) it can be seen that

$$\bar{P} = -\frac{\bar{\theta}_z}{r\rho_0}\nabla_\theta M. \tag{6.4}$$

Using definition (4.1), (6.1) may be written

$$\tilde{P} = -\frac{f}{r|f|}\nabla_\theta M < 0. \tag{6.5}$$

Wherever shears are such that environmental angular momentum increases inward toward the rotation axis along accessible parcel trajectories, a region of anomalous $\tilde{P}$ exists. Regions of anomalous $\tilde{P}$ in Figs. 4c–7c are almost entirely due to meridional shear. They may

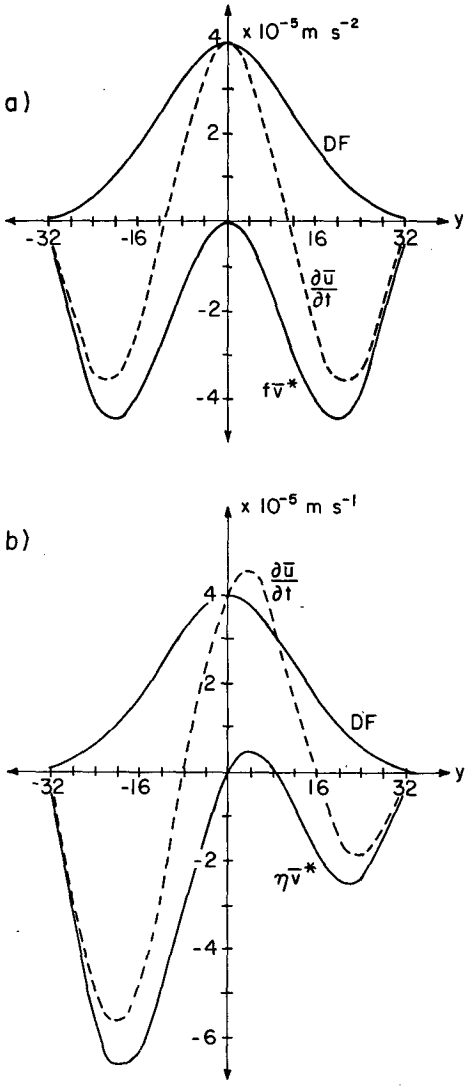

FIG. 19. Expected latitudinal profiles of westerly acceleration (dashed line), given the wave driving profile DF and convergent meridional flow at the equator in the case of (a) no meridional shear and (b) constant northward shear.

thus be appropriately referred to as regions of anomalous absolute vorticity. In such regions displaced parcels will accelerate, the energy coming from the kinetic energy of the zonal flow. Just as convection tends to mix θ to produce a uniform distribution, circulations arising from inertial acceleration would mix M to produce a uniform distribution in a nondissipative atmosphere.

The possible relevance of symmetric inertial instability in the equatorial middle atmosphere came to light with the theoretical work of Dunkerton (1981) and the modeling results of Hunt (1981). Dunkerton found that, in the inviscid case, growing modes exist for any nonzero shear, the growth rates being fastest for the gravest latitudinal mode and shortest vertical scale. He found that a finite vertical scale could be produced by including dissipation. With $N = 0.02$ s^{-1} and $\beta = 2.3 \times 10^{-11}$ m^{-1}-s^{-1}, Dunkerton's dissipative formulae give the cutoff values for inertial stability:

$$L_c \approx 2.4\nu^{2/5} \quad \text{and} \quad \Gamma_c \approx 2.6\nu^{1/5}, \qquad (6.6)$$

where ν is in m^2 s^{-1}, L_c in km, and Γ_c in day^{-1}. Sufficiently strong dissipation ($\Gamma_c > \bar{u}_y$) will eliminate any inertial accelerations. For $\bar{u}_y = \Gamma_c$ modes with $L_z < L_c$ will be dissipated. If $\bar{u}_y > \Gamma_c$ a spectrum of inertial circulations will arise which will mix M until $\bar{u}_y$ is reduced to Γ_c. For the gravest neutral viscous mode, symmetric overturning is expected to occur in a stack of cells, with vertical motions at the boundaries of the region where (6.5) occurs.

Hunt (1981) presented evidence of inertial instability in a GCM. His January case exhibited strong meridional shear, with a region of reduced shear just north of the equator. Between 0° and 16°N in the layer 30–78 km, mean meridional motions occurred in layers of opposite sign separated by 5 km (twice the model resolution), with maximum amplitudes at 62.5 km. At that level (6.1) was satisfied in the band 2.25°–15.75°N. He attributed the greatly inhibited penetration of easterlies into the winter hemisphere to mixing by circulations arising from inertial instability.

Both the appearance and inferred effect of the mesospheric meridional circulations during November–January at low latitudes are somewhat compatible with expectations from inertial instability theory. These circulations are centered about regions of anomalous $\tilde{P}$ (Figs. 5 and 6), are stronger in the winter hemisphere (Fig. 11), and the area-averaged values of $\bar{u}_y \sim 3$ day^{-1} and $L_z \sim 25$ km correspond roughly to values from (6.6) for an eddy viscosity $\nu \sim 100$ m^2 s^{-1}, which might be attributed to breaking gravity waves (Lindzen, 1981). During December–January at 0.5 mb the region 0°–20°N resembles a shelf, with strong meridional shears concentrated at the boundaries (Fig. 13a). The meridional "jet" in Fig. 16 accelerates near 4°N and decelerates near 24°N. Finally, amplification of SAO circulation cells in December coincides with a reduction in $\bar{u}_y$ (Fig. 3a, c).

On the other hand, the poleward extent of the SAO residual circulation cells is ~30°–40°, rather than ~20°, which is the maximum extent of $\tilde{P} \leqslant 0$. This discrepancy increases during December–February. Most importantly, the existence of a region of anomalous $\tilde{P}$ is not a sufficient condition for inertial acceleration. Any wave-driven circulation like that in Fig. 1b will produce similar effects on the mean state, helping to confine easterlies to the summer hemisphere and reduce $\bar{u}_y$. The observed redistribution of M is by no means proof of the importance of inertial acceleration.

If spinup of SAO circulation cells by inertial acceleration does occur, the mechanism is tied to the descending zero-wind line by the coincident maximum in $\bar{u}_y$. The effects are expected to be strongest during December in the mesosphere, where $\bar{u}_y$ is largest and Ri is smallest, and to weaken thereafter as the zero wind line descends into the stratosphere. It is intriguing to note that certain peculiar vertically layered structures in the zonally asymmetric temperature field are observed over the equator (Fig. 2a, Coy and Hitchman, 1984) only when $\tilde{P}$ is negative over a fairly broad region in latitude. This occurs only during November through mid-January in the lower mesosphere. This unusual phenomenon is described in a companion paper (Hitchman et al., 1987).

7. Concluding remarks

Most previous studies have described the evolution of the zonal mean state of the equatorial middle atmosphere in terms of time mean, annual and semiannual components. Here the week-to-week evolution is considered. This approach emphasizes the actual changes that occur, lending insight into which mechanisms are likely to be responsible. Strong week-to-week variations indicate the importance of wave driving. The pattern of radiative heating and inferred residual circulation is consistent with wave driving rather than seasonal changes in solar heating. Deep easterly accelerations implicate meridional advection and wave driving by Rossby and gravity waves. Shallow layers of westerly acceleration that descend with time reflect the influence of vertical advection and wave driving by Kelvin and westerly gravity waves.

Local momentum budgets are strongly modified by advection. The rate of descent of the zero wind line is similar to downward velocities which maintain the accompanying warm anomaly against radiative damping. Observed westerly acceleration is very similar to estimated vertical advection. Maximum penetration of easterlies into the winter hemisphere occurs at the level of maximum cross-equatorial shear, just below the descending zero wind line. Advective circulations responsible for this easterly penetration are organized into circulation cells which extend to midlatitudes, influencing the pattern of zonal mean potential vorticity there. Thus, the low-latitude circulation can be affected

by extratropical Rossby wave driving and higher latitudes can be indirectly affected by wave driving due to vertically propagating equatorial waves. These circulation cells can also be important for tracer transport.

Temperature gradients are detected quite well by the LIMS instrument, as evidenced by the fact that the intense vertical wind shears seen in tropical rocket profiles are reasonably well represented by LIMS geostrophic winds. Rocket profiles support ranges in LIMS temperature and zonal wind of 20 K and 100 m s^{-1} and cross-equatorial shears exceeding 3 day^{-1}. This study provides the first quantitative estimates of the distribution of regions of anomalous gradients of angular momentum. Inertial instability may enhance advection by SAO circulation cells, particularly near the solstice when SAO westerlies begin to descend in the lower mesosphere.

Acknowledgments. We thank Kevin Hamilton, Tim Dunkerton, Alan Plumb, John Gille and Ellis Remsberg for useful conversations. We also thank Tsuguhito Yamasaki for the use of his improved radiative heating algorithm and Marlene Anderson for patiently typing the manuscript. This work is based in part on MHH's Ph.D. dissertation at the University of Washington. This work was supported by NASA under Grant NAGW-471.

REFERENCES

Al-ajmi, D. N., R. S. Harwood and T. Miles, 1985: A sudden warming in the middle atmosphere of the Southern Hemisphere. *Quart. J. Roy. Meteor. Soc.*, **111**, 359–389.

Andrews, D. G., and M. E. McIntyre, 1976: Planetary waves in horizontal and vertical shear: the generalized Eliassen-Palm relation and mean zonal acceleration. *J. Atmos. Sci.*, **33**, 2031–2048.

Angell, J. K., and J. Korshover, 1970: Quasi-biennial, annual, and semiannual zonal wind and temperature harmonic amplitudes and phases in the stratosphere and low mesosphere of the Northern Hemisphere. *J. Geophys. Res.*, **75**, 543–550.

Bailey, P. L., and J. C. Gille, 1986: Inversion of LIMS radiance measurements; an operational algorithm. *J. Geophys. Res.*, **91**, 2757–2774.

Barnett, J. J., 1974: The mean meridional temperature behavior of the stratosphere from November 1970 to November 1971 derived from measurements by the Selective Chopper Radiometer on Nimbus 4. *Quart. J. Roy. Meteor. Soc.*, **100**, 505–530.

Belmont, A. D., D. G. Dartt, and G. D. Nastrom, 1974: Periodic variations in stratospheric zonal wind from 20 to 65 km at 80°N to 70°S. *Quart J. Roy. Meteor. Soc.*, **100**, 203–211.

——, ——, and ——, 1975: Variations of stratospheric zonal winds, 20–65 km, 1961–1971. *J. Appl. Meteor.*, **14**, 585–594.

Boyd, J., 1976: The noninteraction of waves with the zonally-averaged flow on a spherical earth and the interrelationships of eddy fluxes of energy, heat and momentum. *J. Atmos. Sci.*, **33**, 2285–2291.

Chandra, S., 1985: Solar-induced oscillations in the stratosphere: a myth or reality? *J. Geophys. Res.*, **90**, D1, 2331–2339.

Cole, A. E., 1968: Periodic oscillations in the tropical and subtropical atmosphere at levels between 25 and 80 km. *Space Research*, **8**, 823–834.

Coy, L., 1979: An unusually large westerly amplitude of the quasi-biennial oscillation. *J. Atmos. Sci.*, **36**, 174–176.

——, and M. H. Hitchman, 1984: Kelvin wave packets and flow acceleration: A comparison of modeling and observations. *J. Atmos. Sci.*, **41**, 1875–1880.

Crane, A. J., 1979: Annual and semiannual waves in the temperature of the mesosphere as deduced from Nimbus-6 PMR measurements. *Quart. J. Roy. Meteor. Soc.*, **105**, 509–520.

Dunkerton, T. J,, 1981: On the inertial instability of the equatorial middle atmosphere. *J. Atmos. Sci.*, **38**, 2354–2364.

——, 1982: Theory of the mesopause semiannual oscillation. *J. Atmos. Sci.*, **39**, 2681–2690.

——, and D. P. Delisi, 1985: Climatology of the equatorial lower stratosphere. *J. Atmos. Sci.*, **42**, 376–396.

——, C.-P. F. Hsu and M. E. McIntyre, 1981: Some Eulerian and Lagrangian diagnostics for a model stratospheric warming. *J. Atmos. Sci.*, **38**, 819–843.

Edmon, H. J., B. J. Hoskins and M. E. McIntyre, 1980: Eliassen-Palm cross sections for the troposphere. *J. Atmos. Sci.*, **37**, 2600–2616.

Eliassen, A., and E. Kleinschmidt, 1957: Dynamic Meteorology. *Handbrüch der Physik*, Vol. 48, Springer-Verlag, 1–154.

Fels, S. B., and M. D. Schwartzkopf, 1981: An efficient, accurate algorithm for calculating CO_2 15-μ band cooling rates. *J. Geophys. Res.*, **86**, 1205–1232.

Finger, F. G., M. E. Gelman, F. J. Schmidlin, R. Leviton and V. W. Kennedy, 1975: Compatibility of meteorological rocketsonde data as indicated by international comparison tests. *J. Atmos. Sci.*, **32**, 1705–1714.

Gille, J. C., and J. M. Russell III, 1984: The Limb Infrared Monitor of the Stratosphere (LIMS) experiment description, performance, and results. *J. Geophys. Res.*, **89**(D4), 5125–5140.

Gille, J. D., J. M. Russell III, P. L. Bailey, L. L. Gordley, E. E. Remsberg, J. H. Leinesch, W. G. Planet, F. B. House, L. V. Lyjak and S. A. Beck, 1984: Validation of temperature retrievals obtained by the Limb Infrared Monitor of the Stratosphere (LIMS) experiment on Nimbus 7. *J. Geophys. Res.*, **89**, D4, 5147–5160.

Gordley, L. L., and J. M. Russell, 1981: Rapid inversion of limb radiance data using an emissivity growth approximation. *Appl. Opt.*, **20**, 807–813.

——, —— and E. E. Remsberg, 1985: Global lower mesospheric water vapor revealed by LIMS observations. *Atmospheric Ozone, Proc. Quadrennial Ozone Symposium*, Reidel.

Gray, L. G., and J. A. Pyle, 1986: The semiannual oscillation and equatorial tracer distributions. *Quart. J. Roy. Meteor. Sci.*, **112**, 387–407.

Groves, G. V., 1972: Annual and semiannual zonal wind components and corresponding temperature and density variations, 60–130 km. *Planet. Space Sci.*, **20**, 2099, 2112.

Hamilton, K., 1982: Rocketsonde observations of the mesospheric semiannual oscillation at Kwajalein. *Atmos.-Ocean*, **20**, 281–286.

——, 1984: Mean wind evolution through the quasi-biennial cycle in the tropical lower stratosphere. *J. Atmos. Sci.*, **41**, 2113–2125.

Hayashi, Y., D. G. Golder and J. D. Mahlman, 1984: Stratospheric and mesospheric Kelvin waves simulated by the GFDL "SKYHI" general circulation model. *J. Atmos. Sci.*, **41**, 1971–1984.

Hirota, I., 1978: Equatorial waves in the upper stratosphere and mesosphere in relation to the semiannual oscillation of the zonal wind. *J. Atmos. Sci.*, **35**, 714–722.

——, and J. J. Barnett, 1977: Planetary waves in the winter mesosphere—preliminary analysis of Nimbus-6 PMR results. *Quart. J. Roy. Meteor. Soc.*, **103**, 487–498.

Hitchman, M. H., 1985: An observational study of wave-mean flow interaction in the equatorial middle atmosphere. Ph.D. dissertation, University of Washington, 360 pp.

——, C. B. Leovy, J. C. Gille and P. L. Bailey, 1987: Quasi-stationary zonally asymmetric circulations in the equatorial lower mesosphere. Submitted to *J. Atmos. Sci.*

Hopkins, R. H., 1975: Evidence of polar-tropical coupling in upper stratospheric zonal wind anomalies. *J. Atmos. Sci.*, **32**, 712–719.

Hoskins, B. J., M. E. McIntyre and A. W. Robertson, 1986: On the

use and significance of isentropic potential vorticity maps. *Quart. J. Roy. Meteor. Soc.*, **111,** 877–946.

Hunt, B. G., 1981: The maintenance of the zonal mean state of the upper atmosphere as represented in a three-dimensional general circulation model extending to 100 km. *J. Atmos. Sci.*, **38,** 2172–2186.

Kantor, A. J., and A. E. Cole, 1964: Zonal and meridional winds to 120 km. *J. Geophys. Res.*, **69,** 5131–5140.

Koshelkov, Y. P., and A. I. Butko, 1980: Seasonal variations in atmospheric temperature in the Southern Hemisphere at heights of 25–80 km. *Meteor. Gidrol.*, **4,** 12–16.

Labitzke, K., and B. Goretzki, 1982: A catalogue of dynamic parameters describing the variability of the middle stratosphere during the northern winters. *Middle Atmosphere Program Handbook,* Vol. 5, May. SCOSTEP Secretariat, University of Illinois, Urbana, Illinois 61801.

Lindzen, R. S., 1981: Turbulence and stress owing to gravity waves and tidal breakdown. *J. Geophys. Res.*, **86**(C10), 9707–9714.

——, and J. R. Holton, 1968: A theory of the quasi-biennial oscillation. *J. Atmos. Sci.*, **25,** 1095–1107.

McGregor, J., and W. A. Chapman, 1978: Observations of the annual and semiannual wave in the stratosphere using Nimbus-5 SCR data. *J. Atmos. Terres. Phys.*, **40,** 677–684.

McIntyre, M. E., and T. N. Palmer, 1983: Breaking planetary waves in the stratosphere. *Nature,* **305,** 593–600.

Meyer, W. D., 1970: A diagnostic numerical study of the semiannual variation of the zonal wind in the tropical stratosphere and mesosphere. *J. Atmos. Sci.*, **27,** 820–830.

Murgatroyd, R. J., and F. Singleton, 1961: Possible meridional circulations in the stratosphere and mesosphere. *Quart. J. Roy. Meteor. Soc.*, **87,** 125–135.

Nastrom, G. D., and A. D. Belmont, 1975: Periodic variations in stratospheric–mesospheric temperature from 20–65 km at 80°N to 30°S. *J. Atmos. Sci.*, **32,** 1715–1722.

Nestler, M. S., 1983: A comparative study of measurements from radiosondes, rocketsondes, and satellites. NASA Contractor Rep. 168343.

Plumb, R. A., and R. C. Bell, 1982: A model of the quasi-biennial oscillation on an equatorial beta-plane. *Quart. J. Roy. Meteor. Soc.*, **108,** 335–352.

Quiroz, R. S., and A. J. Miller, 1967: Note on the semiannual wind variation in the equatorial stratosphere. *Mon. Wea. Rev.*, **95,** 635–641.

Ramanathan, V., and R. E. Dickinson, 1979: The role of stratospheric ozone in the zonal and seasonal radiative energy balance of the earth–troposphere system. *J. Atmos. Sci.*, **36,** 1084–1104.

Reed, R. J., 1962: Some features of the annual temperature regime in the tropical stratosphere. *Mon. Wea. Rev.*, **90,** 211–215.

——, 1966: Zonal wind behavior in the equatorial stratosphere and lower mesosphere. *J. Geophys. Res.*, **71,** 4223–4233.

Remsberg, E. E., J. M. Russell III, L. L. Gordley, P. L. Bailey, W. G. Planet, and J. E. Harries, 1984a: The validation of Nimbus-7 LIMS measurements of ozone. *J. Geophys. Res.*, **89,** 5161–5178.

——, ——, ——, J. C. Gille and P. L. Bailey, 1984b: Implications of the stratospheric water vapor distribution as determined from the Nimbus 7 LIMS experiment. *J. Atmos. Sci.*, **41,** 2934–2945.

Rodgers, C. D., 1976: Retrieval of atmospheric temperature and composition from remote measurements of thermal radiation. *Rev. Geophys. Space Phys.*, **14,** 609–624.

Salby, M. L., D. L. Hartmann, P. L. Bailey and J. C. Gille, 1984: Evidence for equatorial Kelvin modes in Nimbus-7 LIMS. *J. Atmos. Sci.*, **40,** 220–235.

Solomon, S., J. T. Kiehl, R. R. Garcia and W. Grose, 1986: Tracer transport by the diabatic circulation deduced from satellite observations. *J. Atmos. Sci.*, **43,** 1603–1617.

van Loon, H., K. Labitzke and P. J. Jenne, 1972: Half-yearly waves in the stratosphere. *J. Geophys. Res.*, **77,** 3846–3855.

Wehrbein, W. M., and C. B. Leovy, 1982: An accurate radiative heating and cooling algorithm for use in a dynamical model of the middle atmosphere. *J. Atmos. Sci.*, **39,** 1532–1544.

Yamasaki, T., 1987: A detailed radiative heating algorithm for use with middle atmospheric satellite data. M.S. thesis, University of Washington.